Lasing by Template-Assisted Self-Assembled Quantum Dots

Olha Aftenieva, Markas Sudzius, Anatol Prudnikau, Mohammad Adnan,
Swagato Sarkar, Vladimir Lesnyak, Karl Leo,* Andreas Fery,* and Tobias A.F. König*

Miniaturized laser sources with low threshold power are required for integrated photonic devices. Photostable core/shell nanocrystals are well suited as gain material and their laser properties can be exploited by direct patterning as distributed feedback (DFB) lasers. Here, the 2nd-order DFB resonators tuned to the photoluminescence wavelength of the QDs are used. Soft lithography based on template-assisted colloidal self-assembly enables pattern resolution in the subwavelength range. Combined with the directional Langmuir–Blodgett arrangement, control of the waveguide layer thickness is further achieved. It is shown that a lasing threshold of 5.5 mJ cm^{-2} is reached by a direct printing method, which can be further reduced by a factor of ten (0.6 mJ cm^{-2}) at an optimal waveguide thickness. Moreover, it is discussed how one can adjust the DFB geometries to any working wavelength. This colloidal approach offers prospects for applications in bioimaging, biomedical sensing, anti-counterfeiting, or displays.

O. Aftenieva, M. Adnan, S. Sarkar, A. Fery, T. A. F. König
Leibniz-Institute of Polymer Research Dresden e. V.
Hohe Straße 6, 01169 Dresden, Germany
E-mail: fery@ipfdd.de; koenig@ipfdd.de

M. Sudzius, K. Leo
Dresden Integrated Center for Applied Physics and Photonic Materials
(IAPP)
Technische Universität Dresden
01069 Dresden, Germany
E-mail: leo@iapp.de

A. Prudnikau, V. Lesnyak
Institute of Physical Chemistry
Technische Universität Dresden
Zellescher Weg 19, 01069 Dresden, Germany

M. Adnan
Physikalisches Institut
Westfälische Wilhelms-Universität Münster
Wilhelm-Klemm-Straße 10, 48149 Münster, Germany

K. Leo, A. Fery, T. A. F. König
Center for Advancing Electronics Dresden (cfaed)
Technische Universität Dresden
01062 Dresden, Germany

A. Fery
Chair for Physical Chemistry of Polymeric Materials
Technische Universität Dresden
Mommsenstr. 4, D-01062 Dresden, Germany

The ORCID identification number(s) for the author(s) of this article can be found under https://doi.org/10.1002/adom.202202226.

1. Introduction

The continuing miniaturization of the on-chip devices requires compact semiconductor light sources that are tunable and can operate at a minimal energy input.[1] Colloidal semiconductor quantum dots (QDs), where the bandgap can be easily adjusted within a broad energy range by changing their size, shape, and material composition, are therefore promising candidates as a gain component in such miniaturized devices.[2] Utilizing colloidal QDs allows for cost-efficient wet-chemical processing and is independent of the limitations of the substrate-preferential growth in conventional semiconductor lasers.[3–5] The high standards in synthesizing colloidal QDs result in improved photostability and outstanding optical gain, bringing QDs-based lasers closer to practical applications and circuit integration.[6] Moreover, constructing heteronanocrystals and combining several semiconductor materials provide additional flexibility in engineering their physical and chemical properties.[7] In particular, core/shell nanocrystals, comprised of cadmium selenide and zinc cadmium sulfide (CdSe/ZnCdS), feature large exciton volumes and strong quantum confinement that significantly decrease the Auger recombination rate.[8,9] The ZnCdS shell passivates the surface of the CdSe core, increasing the photoluminescence (PL) quantum yields (PLQY) via suppression of nonradiative exciton recombination, and, at the same time, controls the energy transfer between closely packed QDs, improving the overall device performance.[10]

Up to date, optically pumped lasers featuring semiconductor colloidal QDs were already successfully realized through various resonator configurations: in Fabry–Perot cavities,[11–13] through whispering-gallery modes (WGM) in microrings,[14–17] microdisks[18–20] and microspheres,[21–24] in vertical external cavities,[25,26] distributed feedback (DFB),[27] integrated into photonic crystals[28,29] or combined with plasmonic lattices.[30–33] Looking from the fabrication perspective, the earliest works already demonstrated lasing from the so-called coffee-rings of QDs, formed after drop-casting and drying the colloidal solution on a substrate.[34] Such an approach, however, suffers from size and shape limitations and provides poor positioning accuracy. Thus, high-precision micro- and nanofabrication techniques came into view in recent years. In this regard, the most robust and well-controllable configuration is a DFB resonator that consists of a 2D planar thin-film waveguide combined with a diffractive structure.[35] The periodicity of the diffractive structure p must obey the Bragg condition: $m \cdot \lambda_{Bragg} = 2 \cdot p \cdot n_{eff}$;

**ADVANCED
SCIENCE NEWS**

www.advancedsciencenews.com

**ADVANCED
OPTICAL
MATERIALS**

www.advopticalmat.de

where m is the diffraction order, λ_{Bragg} is the so-called Bragg resonant wavelength, and n_{eff} is the effective refractive index of the propagating mode.[36] For the DFB structures, based on the 1st order diffraction, where m is equal to 1, both the optical feedback and the output are provided by the 1st diffracted order, propagating in the plane of the waveguide layer. Even though it is preferable for integrated photonics applications, extracting light from such configurations remains challenging.[37] As an alternative, 2nd diffraction order can be exploited. While it propagates in-plane and provides the feedback, the 1st order propagates perpendicularly to the plane of the grating, enabling the light output. Such structures, even though being impaired by higher lasing thresholds compared to 1st-order gratings, create efficient surface-emitting lasers.[38–41] In this regard, careful design of the resonator geometry plays a crucial role. The effective refractive index n_{eff} depends on the mode profile of the propagating mode and is directly connected to the thickness of the thin-film waveguide under the grating.[42] Thus, to match the Bragg resonant wavelength to the PL of the QDs, the periodicity of grating has to be adjusted to the thickness of the waveguide-like layer and material properties of the QDs. The manufacturing strategies must provide, therefore, sufficient control over both geometrical parameters.

Up to now, most of the QDs-based DFB nanolasers were produced by depositing colloids onto a structured substrate.[43–55] Being relatively straightforward, such an approach relies on elaborated substrate preparation and does not allow for creating multicomponent systems. To circumvent that, various direct micro- and nanopatterning techniques were introduced, such as template stripping,[56] electron-beam lithography (EBL),[57–60] laser ablation,[61] photolithography on the blends of QDs and photosensitive polymer[62,63] or nanoimprinting of the composites of QDs and high-refractive index-matrixes.[64] Still, most of these methods either rely on templates produced with EBL that highly increase manufacturing costs or require the presence of bulk polymers, impeding the inter-particle coupling and reducing the mode confinement.[57] As an alternative, confinement self-assembly (CSA)[65,66] based on laser interference lithography (LIL)[67] can be applied to arrange colloidal QDs with the help of soft structured molds.[68] In contrast to other template-assisted assembly techniques, CSA allows for multi-cycle production with a single soft polymer stamp,[67] whereas LIL reduces the overall manufacturing costs.[69] This approach was already successfully employed for perovskite nanocrystals, resulting in uniform metasurfaces over macroscopic areas with nanometer-resolved diffractive features.[70] The presence of the sub-micron structuring itself induces the amplification of the emitted light, but can only cause lasing if carefully matched with the guided modes in the layer underneath.[71,72] Thus, the nanometer-precise thickness of the waveguide layer under the grating requires additional effort. To achieve control down to a monolayer of closely packed colloidal QDs and, at the same time, achieve thickness values enough to sustain guided modes, Langmuir–Blodget layer-by-layer (LbL) deposition can be applied.[73,74] Other thin film deposition techniques, such as drop-casting,[75] spin-coating,[76] jet spraying,[77] or electrophoretic deposition[78] cannot provide sufficient control over the thickness and are accompanied by significant material waste.

In this work, we provide a rational design approach to develop self-assembled colloid-based laser structures featuring 2nd order DFB resonator. Taking into account the material properties of the gain material, we employ detailed numerical simulations to find the optimal geometrical configuration of the DFB resonator, namely, the periodicity of the diffractive structure and the thickness of the guided mode layer. The optimized metasurfaces were manufactured with the help of soft lithography-based CSA, taking advantage of submicron resolution for the grating component. By combining CSA with the Langmuir–Blodgett deposition, we can achieve additional control over the thickness of the waveguide component. We achieve efficient light amplification in the lasing regime and characterize the transition from spontaneous to stimulated emission within a broad range of pump powers. The suggested approach allows for manufacturing nanolasers in a controlled, cost-efficient way over centimeter-scaled areas bringing such colloidal light-emitting metasurfaces one step closer to integrated optoelectronic device applications.

2. Results and Discussion

We performed the geometry optimization of the 2nd-order DFB configuration with the help of finite difference time domain (FDTD) analysis (see Figure S1, Supporting Information). To create a realistic representation of the gain medium, we implemented the dispersive material properties of the CdSe/ZnCdS QDs into the numerical simulations (Figure S2, Supporting Information). The Bragg condition was satisfied by tuning the geometrical parameters of the DFB structure, depicted in **Figure 1**a, namely, its periodicity – p and thickness of the waveguiding layer – h. In this way, the highest spectral overlap of the guided mode and the PL spectrum of the gain medium was achieved, maintaining its quality factor of Q $\approx$ 300. Figure 1b shows a transmission spectrum (T) of a metasurface with exemplary periodicity $p = 430$ nm and height $h = 140$ nm under the broadband polarized illumination with the electric (E) field vector parallel to the grating lines. It supports a narrow-bandwidth transverse electric (TE) mode, satisfying the Bragg condition and matching the PL maximum of a thin film of CdSe/ZnCdS QDs at 650 nm (see Figure S3, Supporting Information). We illustrated the necessity of a structured surface over a waveguiding layer through the E-field maps at a resonant wavelength: efficient energy confinement is reflected through the E-field intensity located at the positions of 1D grating lines (Figure 1c). First, we performed a comprehensive parameter sweep to determine the modes with the highest quality (Q) factor: in Figure 1d, it corresponds to the brightest color. The Q factor, defined by the peak position and spectral width quotient, is calculated from the transmission spectrum. Then, by taking into account the mode wavelength, it was correlated with the emission spectrum, defining the region of interest for the considered geometrical parameters. The color map in Figure 1e shows the deviation of the resonant peak from the PL maximum of a flat film at 650 nm: with the nearest modes featuring the brightest color. The Q factor of each mode was then multiplied by the ratio of the PL intensities at the resonant peak position and 650 nm. In such a way, by scaling the
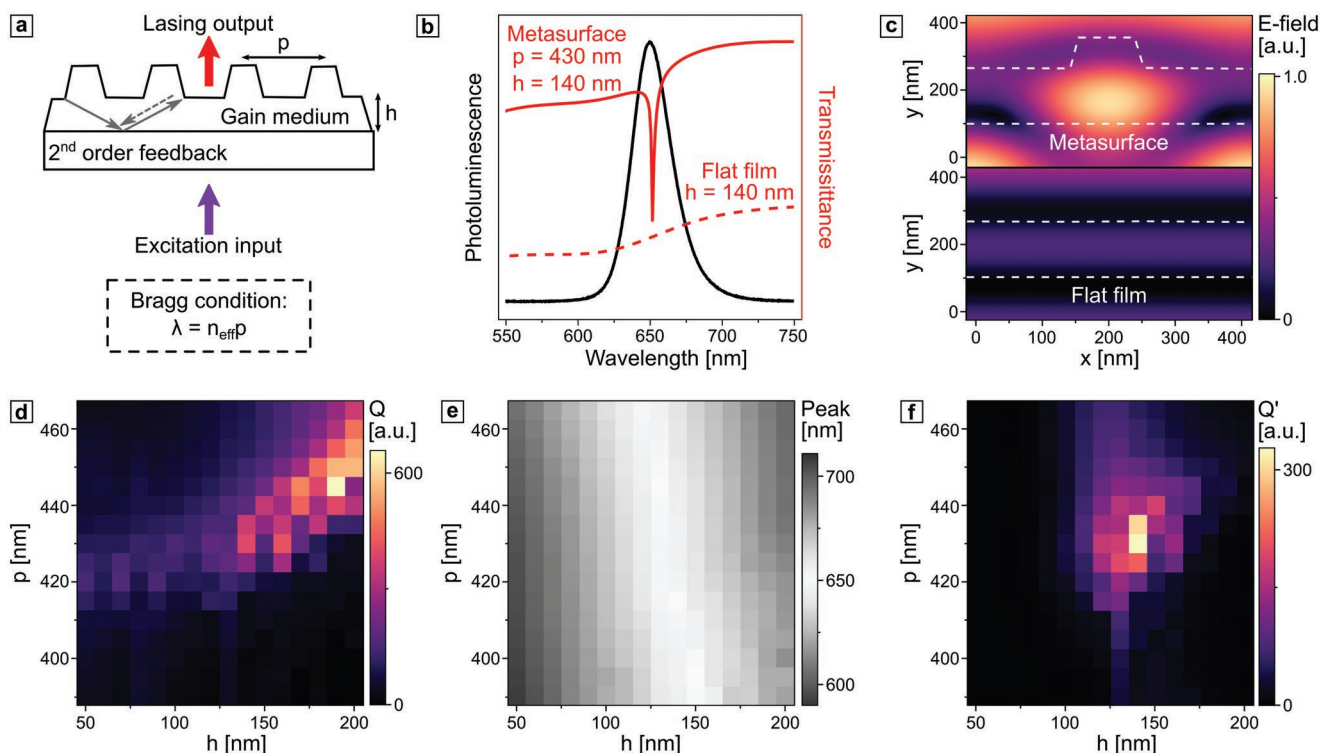
Figure 1. a) Schematic representation of the device structure, fulfilling the 2nd order Bragg condition. b) Simulated transmission spectra for the device geometry and a flat film with the same layer thickness under broadband TE-polarized excitation. The black line denotes CdSe/ZnCdS PL spectrum with a peak at 650 nm. c) The corresponding calculated E-field profiles under 650 nm TE-polarized resonance condition. d) Simulated dependence of the Q factor of the guided mode and e) its spectral position on the grating periodicity and the waveguide layer thickness. f) Parameter sweep map for the scaled Q' factor. The optimization, aimed at maximizing the optical quality, was performed by mapping the Q factors (d) to the peak position distribution (e), where the 650 nm was taken as a maximum normalizing value.

Q factor by the relative spectral position of the mode, we identified the optimal geometrical parameters: $p = 428$–438 nm and $h = 140$ nm, accounting for both: the narrow bandwidth of the guided mode, and its spectral match to the PL spectrum.

2.2. Fabrication via Soft Lithography-Based Confinement Self-Assembly and Langmuir–Blodgett Layer-by-Layer Deposition

Periodicity and layer thickness are two critical geometrical parameters that determine the optical quality of the structure. The confinement self-assembly by tailored polydimethylsiloxane (PDMS) molds allows for robust and reproducible manufacturing of the grating structures with a fixed periodicity. In contrast, we can obtain only an exact layer thickness adjustment by sequential deposition of QD monolayers. Next, we will compare the LbL fabrication method with a simple direct printing method. For the direct printing approach, a highly concentrated (≈110 mg mL^{-1}) colloidal solution of CdSe/ZnCdS QDs in chloroform, capped with oleic acid (OA), was confined between the structured PDMS template and a glass substrate. Upon drying, it was assembled into a periodic 1D grating, residing on a waveguide-like layer depicted in **Figure 2**a. The structured layer was formed over centimeter-scaled areas, as demonstrated in Figure 2b. The surface characterization with scanning electron and atomic force microscopy (SEM and AFM) techniques

revealed the anticipated colloidal metasurface. As mentioned, such a direct printing approach, performed in organic solvents and at high concentrations of nanocrystals, turns out to be challenging in terms of controlling the thickness of the waveguide-like layer under the periodic pattern. Here, the average thickness within the area of interest reached a sub-optimal value of ≈80 nm, being, nevertheless, still sufficient to sustain a guided mode.

On the other hand, to produce the structure with the calculated design parameters, one must build the waveguide layer stepwise using the LbL approach. For this purpose, the surface properties of QDs were modified using the ligand exchange procedure to ensure their selective solubility in various solvents. The successful ligand exchange was confirmed by Fourier-transform infrared spectroscopy measurements of well-purified QDs (Figure S4, Supporting Information). After the ligand exchange, the colloidal QDs capped with OA were soluble in chloroform and octane. In contrast, QDs capped with 2-(2-methoxyethoxy) acetic acid (MEAA) were also soluble in chloroform but insoluble in octane. The MEAA-capped QDs in chloroform were deposited with the help of a Langmuir–Blodgett method, depicted in **Figure 3**a. After transferring the film, formed through drop-casting the colloidal solution on the water-air interface from water to a glass substrate, its thickness was measured with the help of AFM, revealing a ≈7 nm-thick film (see Figure S5, Supporting Information). This value
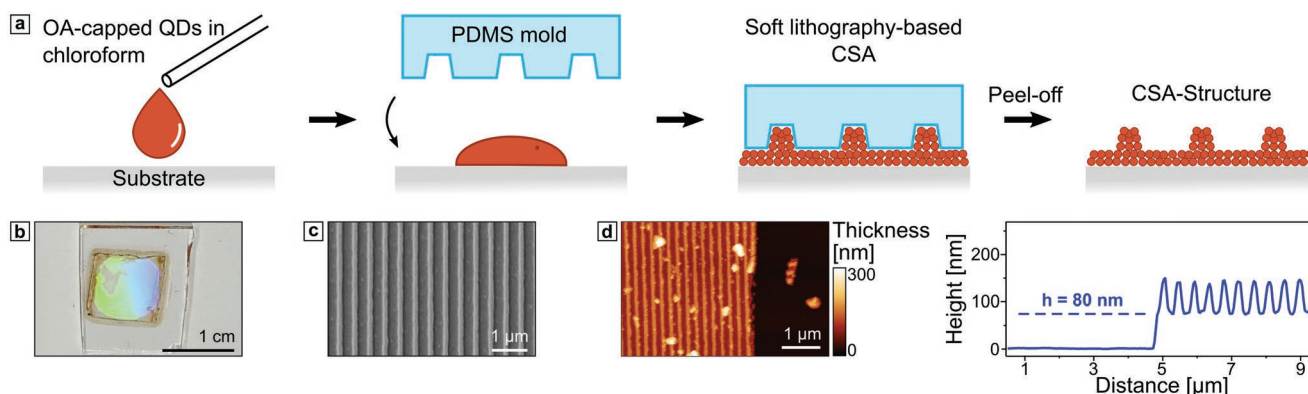
2202226 (3 of 9)

Figure 2. a) Schematic representation of the CSA technique. b) Photograph of an imprinted metasurface with the periodicity of the 1D pattern $p = 435$ nm. c) SEM and d) AFM micrographs of the fabricated structure with the height profile taken across the grating lines.

matched the average diameter of the CdSe/ZnCdS QDs of ≈6.5 nm, indicating a single-particle monolayer formation. We repeated this procedure 22 times until we reached the desired thickness. Then, we applied the CSA to the colloidal solution of QDs, capped with OA and dispersed in octane. Since MEAA-capped QDs are insoluble in octane, the underlying layer of QDs remained intact. For this assembly step, the colloidal solution was diluted down to 5 mg mL^{-1} to avoid residual thin film formation under the 1D grating pattern.

The detailed surface characterization of the produced structure (Figure 3d) also revealed a more granular morphology of the waveguide layer than the one made in a one-step imprinting process. We can associate this granular morphology to the LbL transfer process and the ruptures of the monolayer integrity upon drying (see Figure S5, Supporting Information). These

morphological imperfections are smaller than the grating pitch and, therefore, barely influence the emissive and lasing characteristics of the device.

2.3. Optical Characterization and Non-Linear Light Amplification Behavior

We successfully produced the QDs-based DFB setup matching all calculated optical parameters and a structure that partially met the resonance conditions by utilizing the one-step CSA or LbL-supported approaches. The latter, featuring the 80 nm thickness of the waveguide, was produced by a simple one-step CSA process. A two-step procedure that included the LbL deposition based on a Langmuir–Blodgett method revealed the
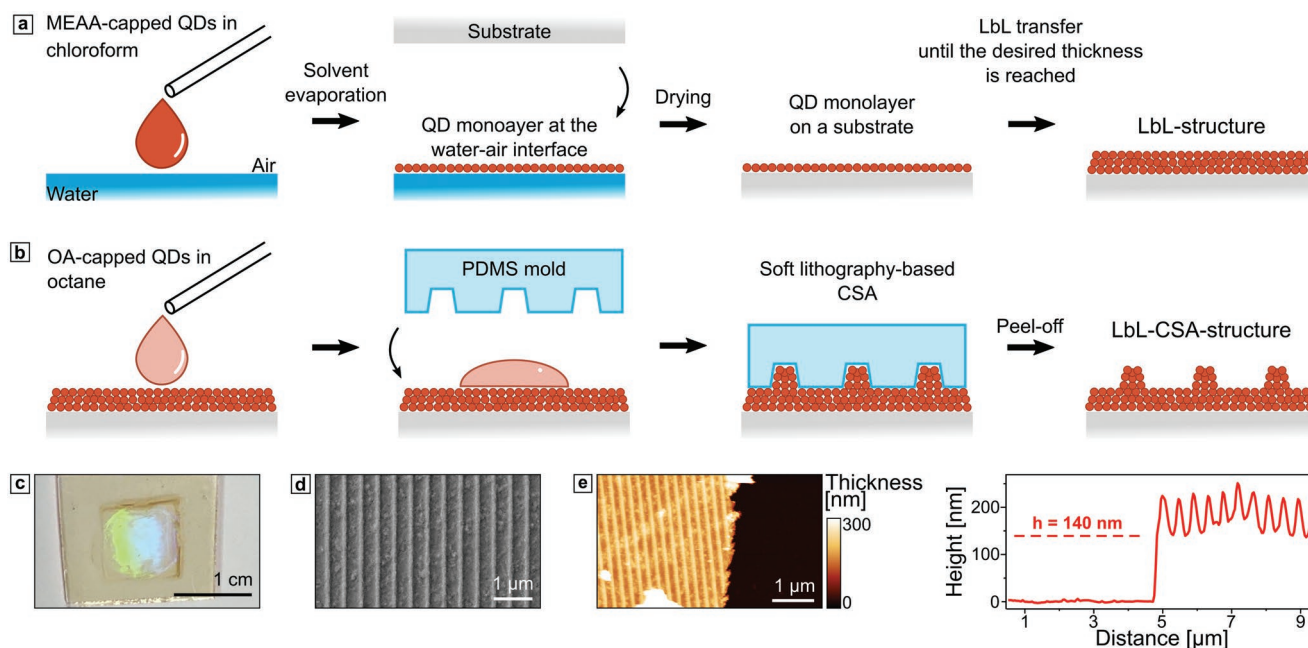

Figure 3. Schematic representation of the a) LbL and b) CSA method applied to 110 mg mL^{-1} of QDs in chloroform and 5 mg mL^{-1} of QDs in octane, respectively. c) Photograph of an imprinted metasurface with the periodicity of the 1D pattern $p = 430$ nm. d) SEM and e) AFM micrographs of the fabricated structure with the height profile taken across the grating lines.
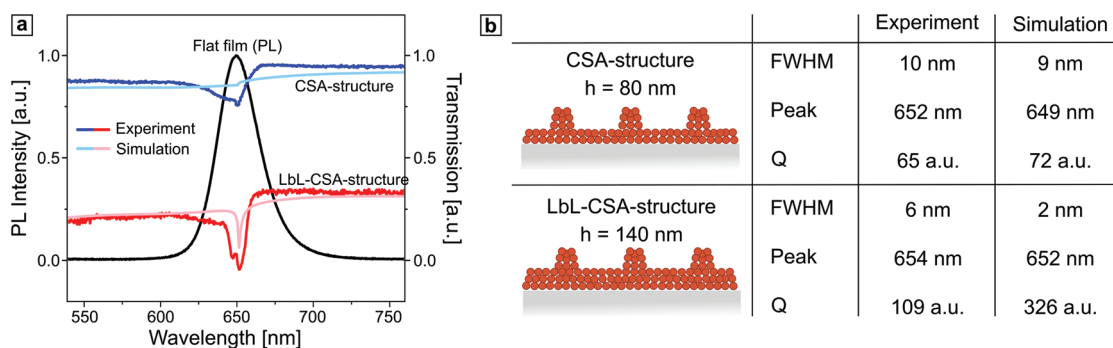
Figure 4. a) Experimental and simulated transmission spectra of the structures with two different thicknesses of the waveguide layer: 80 nm (light blue and blue lines) and 140 nm (light red and red lines). The black line denotes CdSe/ZnCdS PL spectrum. b) Comparative characteristic of the guided modes.

optimal geometrical configuration with the 140-nm-thick waveguide. The transmission spectra of both structures showed a characteristic waveguiding behavior (**Figure 4**). We can observe a narrow-bandwidth dip for both structures at the anticipated wavelength under broad-wavelength TE-polarized illumination. Figure 4a also depicts the simulated transmission spectra for both waveguiding structures, demonstrating the spectral match with the experimental data. We can explain the discrepancy between simulated and experimental data in mode bandwidth and the presence of additional minima by mismatching between the incident polarization (or angle of incidence) and the grating structure. Furthermore, additional scatter may be responsible for this, which we also investigated using a detailed peak analysis (see Figure S6, Supporting Information).

These high-quality guided modes now allow optical pumping and the characterization of laser properties. We recorded the emission spectra of both structures under the femtosecond excitation laser at room temperature in an ambient air environment. The pump beam was projected onto the sample with a spot size of 120 μm, and the emission spectra were recorded after filtering the excitation wavelengths. Notably, no apparent degradation of the gain medium was observed even after 1.5 million excitation cycles at 404 nm and with a 5 kHz repetition rate corresponding to ≈5 min of continuous femtosecond optical pumping that corroborates with the high photostability of the utilized core-shell QDs (Figure S7,

Supporting Information). **Figure 5**a shows the PL spectra at low excitation power, featuring the clear presence of the waveguided modes that split into two PL peaks near the intensity maximum at 650 nm. Figure 5b shows the emission spectra above lasing threshold, with the spectral linewidth below 1 nm. The observed drastic spectral narrowing of the mode from 35 to 1 nm around the lasing threshold unambiguously proves the buildup of coherence in the transitional region from spontaneous to stimulated light emission regime. The input–output curves in Figure 5c demonstrate the characteristic s-shape of the transition from the spontaneous emission regime (left side of the curve) to the stimulated emission process (right side of the curve). The kink in the curve shape is associated with the lasing threshold, indicating the onset of lasing operation mode. We can identify both structures' lasing thresholds at 0.6 and 5.5 mJ cm^{-2} for an LbL-CSA and a CSA structure, respectively. The lower lasing threshold in the LbL-CSA structure is due to preeminent resonator geometry and better light confinement. The difference in optical quality in these two systems could already be seen from the comparison of linear transmission spectra in Figure 4a. On the other hand, in the input–output lasing characteristics in Figure 5c, the better optical confinement in the LbL-CSA structure not only leads to a reduction of the lasing threshold by almost one order of magnitude but also causes a smoother transition from spontaneous to stimulated light emission regime.[79,80] This low threshold pump fluence is
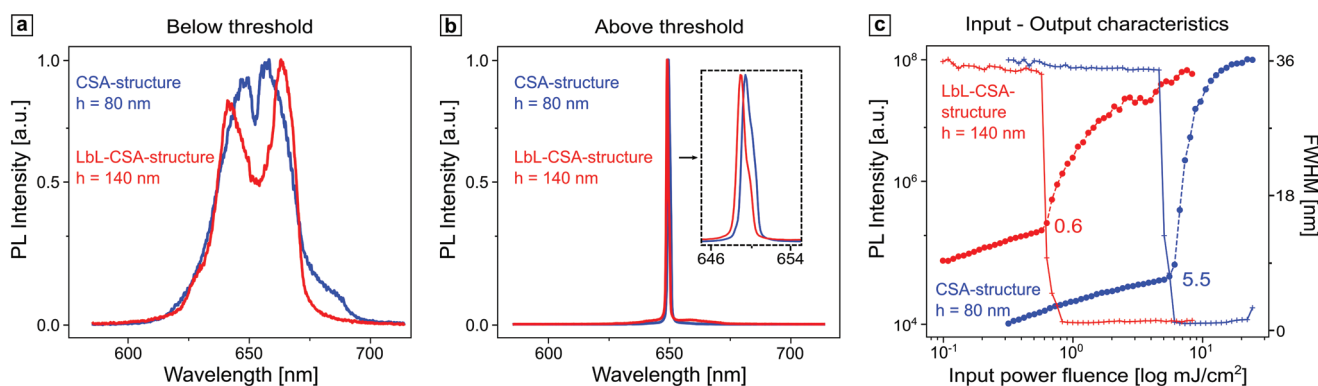

Figure 5. PL spectra of the structure produced via CSA (blue line) and LbL-CSA (red line) methods a) below and b) above the lasing threshold. c) The input–output characteristics of both setups.

**ADVANCED
SCIENCE NEWS**

www.advancedsciencenews.com

**ADVANCED
OPTICAL
MATERIALS**

www.advopticalmat.de

comparable to the existing 2nd order DFB lasers, with colloidal core/shell Cd-chalcogenide-based QDs as a gain medium. For comparison, we have listed in Table S1 (Supporting Information) literature values of laser thresholds with the fabrication methods. Alternative techniques that yield yet lower thresholds rely on the elaborated preparation of a structured substrate. In contrast, the presented method allows for manufacturing efficient lasing devices at low costs and with the possibility to up-scale.

3. Conclusion

This work demonstrates the non-linear amplification of the emitted light from patterned metasurfaces, featuring the 2nd order DFB resonant structure. We employed the directed assembly approach to self-assemble highly luminescent core/shell QD building blocks into 1D gratings on a waveguide layer. Soft CSA allowed for submicron resolution of the periodic lattice, while LbL deposition enabled thickness control of the waveguide down to the size of a single QD. We realized the nanolaser on a centimeter-scale at a low cost and without a separately manufactured structured substrate. We could achieve a significant decrease in the lasing threshold when optimizing the DFB resonators' geometrical parameters. Besides controlling the periodicity of the grating and the thickness of the layer under it, one can explore the effect of pitch width and the depth of the grating lines, including the additional degrees of freedom in the rational design. The combination of soft CSA and LbL deposition enables the manufacture of the required structures quickly and cost-effectively, taking advantage of the tunability of the pattern geometry through LIL.[81] Utilizing core/shell QDs as building blocks brought an additional benefit to the laser operation in ambient conditions. In contrast to organic-inorganic perovskite-based nanolasers, the proposed configuration demonstrated low-threshold lasing without encapsulation or extreme cooling.[82] Taking advantage of the purely colloidal approach, we pave the way to an electrically pumped light-emitting system by replacing the utilized gain medium with suitable colloidal QDs.[83]

4. Experimental Section

Synthesis of Quantum Dots—Chemicals: Cadmium oxide (CdO, 99.99%), 1-octadecene (ODE, 90%), myristic acid (98.5%), oleic acid (OA, 90%), 2-ethylhexanoic acid (≥99%), chloroform (CHCl₃, ≥99%), triethylene glycol dimethyl ether (99%), 2-[2-(2-methoxyethoxy)ethoxy] acetic acid (MEAA, technical grade), octane (98%), and thiourea (99%) were purchased from Sigma–Aldrich. Selenium powder (Se, mesh 160, 99.99%) was purchased from Chempur. Ethanol (EtOH, 99.9%), isopropanol (IPA, HPLC grade), and acetonitrile (HPLC grade) were purchased from VWR Chemicals. Zinc 2-ethylhexanoate (≈80% in mineral spirits (17–19% Zn)) was purchased from Alfa Aesar. All reagents were used as received without further purification.

Synthesis of Quantum Dots—Synthesis of CdSe/ZnCdS Core/Shell QDs: The synthesis was carried out using a standard Schlenk-line technique. First, 2 mmol of CdO (256.8 mg), 5.3 mmol of myristic acid (1.21 g), and 24 mL of ODE were degassed at room temperature for 15 min. After filling the flask with Ar, the mixture was heated up to 270 °C until the CdO fully dissolved to yield a clear, colorless solution. Then the

mixture was cooled down to 90 °C and degassed at this temperature for 2 h to remove water, filled with argon, and the temperature was increased to 240 °C. Then, 1 mmol of Se powder (79 mg) suspended in 1 mL of ODE by ultrasonication for 5 min was quickly injected. The solution was kept for 7 min at this temperature for CdSe QDs growth. Then, the heating mantle was removed, and when the temperature was decreased to 180 °C, 1 mL of 2-ethylhexanoic acid and 2 mL of OA were added to the reaction mixture. After 10 min of stirring, the mixture was heated up to 190 °C, and 2.5 mL of the mixture of Zn- and S-precursor solutions was added dropwise (3 mL h⁻¹) into the reaction flask for the shell growth. (The mixture of Zn- and S-precursor solutions was prepared by dissolving 5.5 mmol (418.7 mg) of thiourea in 7 mL of triethylene glycol dimethyl ether (using ultrasonication) and mixing with 2.52 mL of zinc 2-ethylhexanoate in mineral spirits. The mixture was bubbled with Ar before use.) Then, 0.7 mL of the Cd-precursor solution (prepared by dissolving 128.4 mg (1 mmol) of CdO in 1 mL (6.25 mmol) of 2-ethylhexanoic acid and 1 mL of ODE under heating in an argon atmosphere) was slowly added in the flask at the speed of 3 mL h⁻¹. In 15 min after injection of the Cd-precursor solution, additiobal 3 mL of the mixture of Zn- and S-precursor solutions were injected at 6 mL h⁻¹. Ten minutes after the complete injection of the second part of the Zn- and S-precursors mixture, the flask was cooled down to 60 °C, and the QDs were precipitated by adding IPA with subsequent centrifugation. The precipitate was dissolved in CHCl₃ and precipitated by adding acetonitrile followed by centrifugation. The last procedure was repeated twice. The precipitate obtained was dried under vacuum, weighed, and dissolved in a required amount of CHCl₃.

Synthesis of Quantum Dots—Ligand Exchange: CdSe/ZnCdS core/shell QDs capped with MEAA. 350 μL of MEAA were added to 1.5 mL of QDs solution in chloroform (100 mg mL⁻¹). The solution was stirred on a hot-plate at 30 °C for 48 h in a closed vial protected from light, followed by precipitation using hexane as a nonsolvent and centrifugation. The precipitate was dissolved in a minimal amount of EtOH and precipitated by adding hexane followed by centrifugation. The obtained precipitate was dispersed in 1360 μL of CHCl₃ for further use.

CdSe/ZnCdS core/shell QDs capped with OA. OA (100 μL) was added to QDs solution (1.5 mL) in chloroform (100 mg mL⁻¹). The solution was stirred at room temperature for 24 h in a closed vial protected from light, followed by precipitation using acetonitrile as a nonsolvent and centrifugation. The precipitate was dissolved in CHCl₃ and precipitated by acetonitrile followed by centrifugation. The obtained precipitate was dispersed in 1.36 mL of octane for further use.

Soft Lithography-Based Confinement Self-Assembly—Laser Interference Lithography: To produce a structured film on the glass substrate, LIL was employed. Before use, microscopy glass slides were divided into pieces (2 × 2 cm) and cleaned with isopropyl alcohol and ultrapure water in a 1:1 ratio by sonication for 20 min at 80 kHz. Positive photoresist (mr-P 1202LIL, micro resist technology GmbH, Germany) diluted with the thinner solution (mat-1050, micro resist technology GmbH, Germany) was spin-coated onto the cleaned and dried under a stream of nitrogen substrate. Optimized spin parameters of 3000 rpm, acceleration of 1000 rpm s⁻¹, and total spin time of 33 s produced a thin film of 70 nm thickness, as confirmed by spectroscopic ellipsometry (RC2-DI, J.A. Woollam Co., Inc.). The coated substrates were baked at 95 °C for 60 s and further exposed to the 325 nm laser with a dose of 12 mJ cm⁻². The backside of the substrate was covered with black adhesive tape to avoid unnecessary reflections. To develop the exposed photoresist, the sample was submerged into the developer (mr-D 374/S, micro resist technology GmbH, Germany) for 2 min, rinsed with ultrapure water, and dried under a stream of nitrogen.

Soft Lithography-Based Self-Assembly—Confinement Self-Assembly: Produced by LIL, the structured film of a photoresist was replicated using an elastomeric silicone kit (Sylgard 184, Dow Chemicals, USA) with a ratio of prepolymer and catalyst of 5:1 to create the PDMS mold. To further increase the rigidity of the stamp, it was subjected to thermal treatment in an oven at 180 °C for 3 h. Such a process reduced the swelling of the PDMS form by chloroform from 125% to 30%.

**ADVANCED
SCIENCE NEWS**

www.advancedsciencenews.com

**ADVANCED
OPTICAL
MATERIALS**

www.advopticalmat.de

The resulting mold was trimmed and attached to the weight of 100 g. In the next step, 10 μL of the colloidal solution of CdSe/ZnCdS QDs, capped with OA and dispersed in chloroform at the concentration of 110 mg mL^{-1} or capped with MEAA and dispersed in octane at the concentration of 5 mg mL^{-1}, was drop-cast on a substrate (cleaned microscopy glass or waveguide-like layer of QDs on glass, pre-assembled with the LbL deposition. The weight and the PDMS mold were placed on the QD dispersion to ensure close contact between the mold and the flat surface. The assembly was dried for 1 h at room temperature and relative humidity of 32%. The stamp was then removed by peeling off. Excess of QDs, adhering to the PDMS stamp, could be removed by rinsing the stamp with a corresponding solvent allowing for the re-usage of the stamp. An additional ultrasonication step was recommended to remove the adhering QDs agglomerates.

Soft Lithography-Based confinement Self-Assembly—Layer-by-Layer Deposition: A volume of ~≈10 μL of colloidal MEAA-capped QDs, dispersed in chloroform, at the concentration of ≈4 mg mL^{-1} was drop-cast onto a liquid–air interface, where the liquid phase comprised of 8.33 μm aqueous solution of sodium dodecyl sulfate (SDS). The presence of surfactant was used to confine the spread of the drop-cast QDs at the interface. The volumes and concentrations were optimized to form a monolayer. After the evaporation of chloroform, the self-assembled monolayer war transferred to a solid support. For this, the substrate was rendered hydrophobic via gas-phase deposition of trichloro(1H,1H,2H,2H-perfluorooctyl)silane (448 931, Sigma–Aldrich) at 60 °C for 3 h. The QDs were then manually transferred onto the substrate via the Langmuir–Blodgett method by submerging it parallel to the liquid-air interface through the self-assembled layer. Due to the hydrophobic nature of the QDs, they were preferentially deposited from the aqueous environment to the hydrophobic support. For the subsequent layer transfers, the residual water drops were dried under the stream of nitrogen. After the first layer deposition, the surface was readily hydrophobic due to the presence of QDs and did not require any additional modification. The assembly was performed in a dark room under UV-lamp illumination to better visualize the QD layer at the interface.

Surface Characterization: Produced line structures were imaged with AFM. The scanning was performed in the tapping mode with silicon nitride probes (typical resonant frequency in the air: 296 kHz). The amplitude set-point was adjusted within the range of 100–200 mV at the scanning frequency of 0.5–1 Hz. For the SEM imaging, NEON 40 FIB-SEM workstation (Carl Zeiss Microscopy GmbH, Oberkochen, Germany), operating at an accelerating voltage (electron high tension) of 1 kV, was used.

Ellipsometry: To determine the refractive index of the thin QD films, spectroscopic ellipsometry was performed in the wavelength range from 193 to 1690 nm (combined Deuterium/Quartz-Tungsten Halogen lamps) using a spectroscopic ellipsometer (RC2-DI, J.A. Woollam Co., Inc.). The data were acquired in a reflection mode at various angles of incidence ranging from 45° to 75° in five-degree steps. Si with native oxide layer material data was utilized to model the refractive index of the substrate. To determine the refractive index of CdSe/ZnCdS, a general oscillator layer model was implemented within the CompleteEASE (Version 5.19) software. All modeling approximations complied with Kramers–Kronig relations and showed a mean square error (MSE) below four.

Finite-Difference Time-Domain Simulations: A commercial-grade simulator based on the FDTD method was used to perform the calculations (FDTD: 2D electromagnetic simulator).[84] A plane-wave source was used to simulate the optical response, illuminating the structure at a normal incidence with a polarization angle of 90° representing the TE-polarized light (in-line with the grating lines). The broadband illumination (400–900 nm) was used to collect the transmission. For simulating the E-field distribution, the excitation wavelength was selected according to the emission maximum with a pulse length of 25 ps. Perfectly matching layer boundary conditions were used in the Y-direction, and periodic boundary conditions were used along the X-axis. The grating lines were represented by trapezoids resembling the experimentally measured grating profiles. To obtain the optical responses of the system, frequency-domain field monitors were used. The dielectric properties of CdSe/ZnCdS were imported from the experimentally measured optical constants. For the best simulation stability, the mesh area was set around the existing structure in all two principal directions with a mesh step size of 5 nm, and the auto-shutoff level was set to 10^{-6}. The refractive index substrate was set to 1.5, while the surrounding refractive index was set to 1.

Transmission Spectroscopy: The transmission spectroscopy measurements were performed with a Fourier microscopy setup (NT&C, Germany). The sample was illuminated (illumination spot size ≈100 μm) by a tungsten-halogen light source through a bright-field condenser (LWD, numerical aperture (NA) 0.52, Nikon, Japan), avoiding the ambient light. The back focal plane image (Fourier image) was guided inside the microscope objective (CFI S Plan Fluor ELWD 40X, NA 0.6, Nikon, Japan) into the entrance slit of the spectrometer (IsoPlane 160, Princeton Instruments, USA), opened up to 50 μm. The transmission spectrum was directly collected at a 0° angle of detection and corrected by subtracting the dark current at the detector and normalizing it against the reference spectra collected from an empty glass substrate.

Lasing Threshold and Input–Output Curve Measurement: The samples were excited optically to the absorption band of CdSe/ZnCdS by femtosecond laser pulses with a duration of 100 fs and a repetition rate of 5 kHz. The pulses were produced with a Micra femtosecond oscillator and amplified with a regenerative amplifier Legend Elite Duo, both by Coherent. The second harmonic was generated at 400 nm from the fundamental harmonic output of the regenerative amplifier. The excitation beam was focused by a lens to a spot size of 120 μm in diameter at the sample position. The emission was collected by a high NA objective lens at the opposite side from excitation and guided into a spectrometer equipped with a cooled charge-coupled device camera.

Supporting Information

Supporting Information is available from the Wiley Online Library or from the author.

Acknowledgements

Conflict of Interest

The authors declare no conflict of interest.

Data Availability Statement

The data that support the findings of this study are available in the supplementary material of this article.

Keywords

[1] X. Zhuang, Y. Ouyang, X. Wang, A. Pan, *Adv. Opt. Mater.* **2019**, *7*, 1900071.

[2] S. Hepp, M. Jetter, S. L. Portalupi, P. Michler, *Adv. Quantum Technol.* **2019**, *2*, 1900020.

[3] C. Wang, B. Wang, K. H. Lee, C. S. Tan, S. F. Yoon, J. Michel, *Opt. Express* **2016**, *24*, 23129.

[4] P. Geiregat, D. Van Thourhout, Z. Hens, *NPG Asia Mater.* **2019**, *11*, 41.

[5] J. Chen, K. Rong, *Mater. Chem. Front.* **2021**, *5*, 4502.

[6] L. Qu, X. Peng, *J. Am. Chem. Soc.* **2002**, *124*, 2049.

[7] C. de M Donegá, *Chem. Soc. Rev.* **2011**, *40*, 1512.

[8] S. Wei, Y. Liu, M. Ma, Y. Wu, L. Huang, D. Pan, *J. Mater. Chem. C* **2018**, *6*, 11104.

[9] F. Di Stasio, J. Q. Grim, V. Lesnyak, P. Rastogi, L. Manna, I. Moreels, R. Krahne, *Small* **2015**, *11*, 1328.

[10] X. Wang, J. Yu, R. Chen, *Sci. Rep.* **2018**, *8*, 17323.

[11] M. Li, M. Zhi, H. Zhu, W.-Y. Wu, Q.-H. Xu, M. H. Jhon, Y. Chan, *Nat. Commun.* **2015**, *6*, 8513.

[12] C. Dang, J. Lee, C. Breen, J. S. Steckel, S. Coe-Sullivan, A. Nurmikko, *Nat. Nanotechnol.* **2012**, *7*, 335.

[13] R. K. Patel, A. A. P. Trichet, D. M. Coles, P. R. Dolan, S. M. Fairclough, M. A. Leontiadou, S. C. E. Tsang, D. J. Binks, E. Jang, H. Jang, R. A. Taylor, J. M. Smith, *Adv. Opt. Mater.* **2016**, *4*, 285.

[14] B. le Feber, F. Prins, E. De Leo, F. T. Rabouw, D. J. Norris, *Nano Lett.* **2018**, *18*, 1028.

[15] K. Rong, H. Liu, K. Shi, J. Chen, *Nanoscale* **2019**, *11*, 13885.

[16] M. Zavelani-Rossi, M. G. Lupo, R. Krahne, L. Manna, G. Lanzani, *Nanoscale* **2010**, *2*, 931.

[17] C. Liao, R. Xu, Y. Xu, C. Zhang, M. Xiao, L. Zhang, C. Lu, Y. Cui, J. Zhang, *J. Phys. Chem. Lett.* **2016**, *7*, 4968.

[18] W. Xie, T. Stöferle, G. Rainò, T. Aubert, S. Bisschop, Y. Zhu, R. F. Mahrt, P. Geiregat, E. Brainis, Z. Hens, D. Van Thourhout, *Adv. Mater.* **2017**, *29*, 1604866.

[19] K. Rong, F. Gan, K. Shi, S. Chu, J. Chen, *Adv. Mater.* **2018**, *30*, 1706546.

[20] C. H. Lin, Q. Zeng, E. Lafalce, M. J. Smith, S. T. Malak, J. Jung, Y. J. Yoon, Z. Lin, Z. V. Vardeny, V. V. Tsukruk, *Adv. Opt. Mater.* **2017**, *5*, 1700011.

[21] F. Montanarella, D. Urbonas, L. Chadwick, P. G. Moerman, P. J. Baesjou, R. F. Mahrt, A. van Blaaderen, T. Stöferle, D. Vanmaekelbergh, *ACS Nano* **2018**, *12*, 12788.

[22] P. T. Snee, Y. Chan, D. G. Nocera, M. G. Bawendi, *Adv. Mater.* **2005**, *17*, 1131.

[23] C. Grivas, C. Li, P. Andreakou, P. Wang, M. Ding, G. Brambilla, L. Manna, P. Lagoudakis, *Nat. Commun.* **2013**, *4*, 2376.

[24] Y. Wang, V. D. Ta, K. S. Leck, B. H. I. Tan, Z. Wang, T. He, C.-D. Ohl, H. V. Demir, H. Sun, *Nano Lett.* **2017**, *17*, 2640.

[25] N. Taghipour, S. Delikanli, S. Shendre, M. Sak, M. Li, F. Isik, I. Tanriover, B. Guzelturk, T. C. Sum, H. V. Demir, *Nat. Commun.* **2020**, *11*, 3305.

[26] G. Shan, X. Zhao, M. Hu, C.-H. Shek, W. Huang, *Front. Guided Wave Opt. Optoelectron.* **2012**, *5*, 157.

[27] Y. Wang, S. Chen, Y. Yu, L. Zhou, L. Liu, C. Yang, M. Liao, M. Tang, Z. Liu, J. Wu, W. Li, I. Ross, A. J. Seeds, H. Liu, S. Yu, *Optica, OPTICA* **2018**, *5*, 528.

[28] H. Jung, M. Lee, C. Han, Y. Park, K.-S. Cho, H. Jeon, *Opt. Express* **2017**, *25*, 32919.

[29] H. Chang, K. Min, M. Lee, M. Kang, Y. Park, K.-S. Cho, Y.-G. Roh, S. W. Hwang, H. Jeon, *Nanoscale* **2016**, *8*, 6571.

[30] P.-J. Cheng, Z.-T. Huang, J.-H. Li, B.-T. Chou, Y.-H. Chou, W.-C. Lo, K.-P. Chen, T.-C. Lu, T.-R. Lin, *ACS Photonics* **2018**, *5*, 2638.

[31] C.-Z. Ning, *Adv. Photonics* **2019**, *1*, 014002.

[32] J. Guan, L. K. Sagar, R. Li, D. Wang, G. Bappi, W. Wang, N. Watkins, M. R. Bourgeois, L. Levina, F. Fan, S. Hoogland, O. Voznyy, J. M. de Pina, R. D. Schaller, G. C. Schatz, E. H. Sargent, T. W. Odom, *ACS Nano* **2020**, *14*, 3426.

[33] J. Guan, L. K. Sagar, R. Li, D. Wang, G. Bappi, N. E. Watkins, M. R. Bourgeois, L. Levina, F. Fan, S. Hoogland, O. Voznyy, J. Martins de Pina, R. D. Schaller, G. C. Schatz, E. H. Sargent, T. W. Odom, *Nano Lett.* **2020**, *20*, 1468.

[34] D. Mampallil, H. B. Eral, *Adv. Colloid Interface Sci.* **2018**, *252*, 38.

[35] S. Chénais, S. Forget, *Polym. Int.* **2012**, *61*, 390.

[36] H. Kogelnik, C. V. Shank, *J. Appl. Phys.* **1972**, *43*, 2327.

[37] S. Basak, O. Bar-On, O. Bar-On, J. Scheuer, J. Scheuer, J. Scheuer, *Opt. Mater. Express, OME* **2022**, *12*, 375.

[38] S. Riechel, C. Kallinger, U. Lemmer, J. Feldmann, A. Gombert, V. Wittwer, U. Scherf, *Appl. Phys. Lett.* **2000**, *77*, 2310.

[39] A. E. Vasdekis, G. A. Turnbull, I. D. W. Samuel, P. Andrew, W. L. Barnes, *Appl. Phys. Lett.* **2005**, *86*, 161102.

[40] P. Zhou, L. Niu, A. Hayat, F. Cao, T. Zhai, X. Zhang, *Polymers* **2019**, *11*, 258.

[41] D. Schneider, S. Hartmann, T. Dobbertin, T. Benstem, D. Metzdorf, E. Becker, A. Kammoun, C. Schildknecht, H. Krautwald, H.-H. Johannes, T. Riedl, W. Kowalsky, in *Organic Light-Emitting Materials and Devices VII* (Eds: Z. H. Kafafi, P. A. Lane), International Society For Optics And Photonics, **2004**, pp. 310–317.

[42] D. Marcuse, in *Theory of Dielectric Optical Waveguides*, Academic Press, London **1991**, pp. 97–133.

[43] F. Fan, O. Voznyy, R. P. Sabatini, K. T. Bicanic, M. M. Adachi, J. R. McBride, K. R. Reid, Y.-S. Park, X. Li, A. Jain, R. Quintero-Bermudez, M. Saravanapavanantham, M. Liu, M. Korkusinski, P. Hawrylak, V. I. Klimov, S. J. Rosenthal, S. Hoogland, E. H. Sargent, *Nature* **2017**, *544*, 75.

[44] M. M. Adachi, F. Fan, D. P. Sellan, S. Hoogland, O. Voznyy, A. J. Houtepen, K. D. Parrish, P. Kanjanaboos, J. A. Malen, E. H. Sargent, *Nat. Commun.* **2015**, *6*, 8694.

[45] Y. Zhu, W. Xie, S. Bisschop, T. Aubert, E. Brainis, P. Geiregat, Z. Hens, D. Van Thourhout, *ACS Photonics* **2017**, *4*, 2446.

[46] O. V. Kozlov, Y.-S. Park, J. Roh, I. Fedin, T. Nakotte, V. I. Klimov, *Science* **2019**, *365*, 672.

[47] C. Han, H. Jung, J. Lee, M. Lee, Y. Park, K.-S. Cho, H. Jeon, *Adv. Mater. Technol.* **2018**, *3*, 1700291.

[48] H. Kim, K. Roh, J. P. Murphy, L. Zhao, W. B. Gunnarsson, E. Longhi, S. Barlow, S. R. Marder, B. P. Rand, N. C. Giebink, *Adv. Opt. Mater.* **2020**, *8*, 1901297.

[49] S. Zhang, L.-B. Cui, X. Zhang, J.-H. Tong, T. Zhai, *Opt Express* **2020**, *28*, 2809.

[50] H. Jung, C. Han, H. Kim, K.-S. Cho, Y.-G. Roh, Y. Park, H. Jeon, *Nanoscale* **2018**, *10*, 22745.

[51] F. Todescato, I. Fortunati, S. Gardin, E. Garbin, E. Collini, R. Bozio, J. J. Jasieniak, G. D. Giustina, G. Brusatin, S. Toffanin, R. Signorini, *Adv. Funct. Mater.* **2012**, *22*, 337.

[52] B. Guilhabert, C. Foucher, A.-M. Haughey, E. Mutlugun, Y. Gao, J. Herrnsdorf, H. D. Sun, H. V. Demir, M. D. Dawson, N. Laurand, *Opt Express* **2014**, *22*, 7308.

[53] R. Signorini, I. Fortunati, F. Todescato, S. Gardin, R. Bozio, J. J. Jasieniak, A. Martucci, G. D. Giustina, G. Brusatin, M. Guglielmi, *Nanoscale* **2011**, *3*, 4109.

[54] Y. Gao, L. Y. M. Tobing, A. Kiffer, D. H. Zhang, C. Dang, H. V. Demir, *ACS Photonics* **2016**, *3*, 2255.

[55] T. Zhai, L. Han, X. Ma, X. Wang, *Nanomaterials* **2021**, *11*, 1530.

[56] F. Prins, D. K. Kim, J. Cui, E. De Leo, L. L. Spiegel, K. M. McPeak, D. J. Norris, *Nano Lett.* **2017**, *17*, 1319.

[57] N. Gheshlaghi, S. Foroutan-Barenji, O. Erdem, Y. Altintas, F. Shabani, M. H. Humayun, H. V. Demir, *Nano Lett.* **2021**, *21*, 4598.

[58] T. S. Mentzel, D. D. Wanger, N. Ray, B. J. Walker, D. Strasfeld, M. G. Bawendi, M. A. Kastner, *Nano Lett.* **2012**, *12*, 4404.

[59] Y. Wang, J.-A. Pan, H. Wu, D. V. Talapin, *ACS Nano* **2019**, *13*, 13917.

[60] K. Miszta, F. Greullet, S. Marras, M. Prato, A. Toma, M. Arciniegas, L. Manna, R. Krahne, *Nano Lett.* **2014**, *14*, 2116.

[61] L. Zhang, C. Liao, B. Lv, X. Wang, M. Xiao, R. Xu, Y. Yuan, C. Lu, Y. Cui, J. Zhang, *ACS Appl. Mater. Interfaces* **2017**, *9*, 13293.

[62] S. Myeong, B. Chon, S. Kumar, H.-J. Son, S. O. Kang, S. Seo, *Nanoscale Adv* **2022**, *4*, 1080.

[63] M. J. Smith, C. H. Lin, S. Yu, V. V. Tsukruk, *Adv. Opt. Mater.* **2019**, *7*, 1801072.

[64] C. Pina-Hernandez, A. Koshelev, S. Dhuey, S. Sassolini, M. Sainato, S. Cabrini, K. Munechika, *Sci. Rep.* **2017**, *7*, 17645.

[65] C. Hanske, M. Tebbe, C. Kuttner, V. Bieber, V. V. Tsukruk, M. Chanana, T. A. F. König, A. Fery, *Nano Lett.* **2014**, *14*, 6863.

[66] Y. Yu, C. Ng, T. A. F. König, A. Fery, *Langmuir* **2019**, *35*, 8629.

[67] V. Gupta, S. Sarkar, O. Aftenieva, T. Tsuda, L. Kumar, D. Schletz, J. Schultz, A. Kiriy, A. Fery, N. Vogel, T. A. F. König, *Adv. Funct. Mater.* **2021**, *31*, 2105054.

[68] M. Mayer, M. J. Schnepf, T. A. F. König, A. Fery, *Adv. Opt. Mater.* **2019**, *7*, 1800564.

[69] V. Gupta, O. Aftenieva, P. T. Probst, S. Sarkar, A. M. Steiner, N. Vogel, A. Fery, T. A. F. König, *Advanced Photonics Research* **2022**, *3*, 2200152.

[70] A. Kessel, C. Frydendahl, S. R. K. C. Indukuri, N. Mazurski, P. Arora, U. Levy, *Adv. Opt. Mater.* **2020**, *8*, 2001627.

[71] S. Klinkhammer, X. Liu, K. Huska, Y. Shen, S. Vanderheiden, S. Valouch, C. Vannahme, S. Bräse, T. Mappes, U. Lemmer, *Opt Express* **2012**, *20*, 6357.

[72] V. Navarro-Fuster, I. Vragovic, E. M. Calzado, P. G. Boj, J. A. Quintana, J. M. Villalvilla, A. Retolaza, A. Juarros, D. Otaduy, S. Merino, M. A. Díaz-García, *J. Appl. Phys.* **2012**, *112*, 043104.

[73] O. Erdem, S. Foroutan, N. Gheshlaghi, B. Guzelturk, Y. Altintas, H. V. Demir, *Nano Lett.* **2020**, *20*, 6459.

[74] Y. Justo, I. Moreels, K. Lambert, Z. Hens, *Nanotechnology* **2010**, *21*, 295606.

[75] C. Wang, M. Shim, P. Guyot-Sionnest, *Appl. Phys. Lett.* **2002**, *80*, 4.

[76] Y. Yang, Y. Zheng, W. Cao, A. Titov, J. Hyvonen, J. R. Manders, J. Xue, P. H. Holloway, L. Qian, *Nat. Photon.* **2015**, *9*, 259.

[77] T. C. Nguyen, T. T. T. Can, W.-S. Choi, *Sci. Rep.* **2019**, *9*, 13885.

[78] Y. Aniskevich, A. Radchanka, A. Antanovich, A. Prudnikau, M. T. Quick, A. W. Achtstein, J. H. Jo, G. Ragoisha, M. Artemyev, E. Streltsov, *ACS Appl. Nano Mater.* **2021**, *4*, 6974.

[79] C. Z. Ning, *IEEE J. Sel. Top. Quantum Electron.* **2013**, *19*, 1503604.

[80] M. Sudzius, M. Langner, S. I. Hintschich, V. G. Lyssenko, H. Fröb, K. Leo, *Appl. Phys. Lett.* **2009**, *94*, 061102.

[81] Y. Shimizu, *Nanomanuf. Metrol.* **2021**, *4*, 3.

[82] Z. Li, J. Moon, A. Gharajeh, R. Haroldson, R. Hawkins, W. Hu, A. Zakhidov, Q. Gu, *ACS Nano* **2018**, *12*, 10968.

[83] Y.-S. Park, J. Roh, B. T. Diroll, R. D. Schaller, V. I. Klimov, *Nat. Rev. Mater.* **2021**, *6*, 382.

[84] Nanophotonic FDTD Simulation Software – Lumerical FDTD, https://www.lumerical.com/products/fdtd/ (accessed: June 2022).